Molecules and Cells

Crystal Structures of Spleen Tyrosine Kinase in Complex with Two Novel 4-Aminopyrido[4,3-d] Pyrimidine Derivative Inhibitors

Sang Jae Lee[1,2,5], Jang-Sik Choi[3,5], Seoung Min Bong[1], Hae-Jun Hwang[3], Jaesang Lee[3], Ho-Juhn Song[4], Jaekyoo Lee[4], Jung-Ho Kim[3], Jong Sung Koh[4,*], and Byung Il Lee[1,*]

[1]Research Institute, National Cancer Center, Goyang, Gyeonggi 10408, Korea, [2]The Research Institute of Pharmaceutical Sciences, College of Pharmacy, Seoul National University, Seoul 08826, Korea, [3]Oscotec Inc., Seongnam 13488, Korea, [4]Genosco, 767C Concord Ave, 2nd Floor, Cambridge, MA 02138, USA, [5]These authors contributed equally to this work.
*Correspondence: jskob777@genosco.com (JSK); bilee@ncc.re.kr (BIL)
http://dx.doi.org/10.14348/molcells.2018.2219
www.molcells.org

Spleen tyrosine kinase (SYK) is a cytosolic non-receptor protein tyrosine kinase. Because SYK mediates key receptor signaling pathways involving the B cell receptor and Fc receptors, SYK is an attractive target for autoimmune disease and cancer treatments. To date, representative oral SYK inhibitors, including fostamatinib (R406 or R788), entospletinib (GS-9973), cerdulatinib (PRT062070), and TAK-659, have been assessed in clinical trials. Here, we report the crystal structures of SYK in complex with two newly developed inhibitors possessing 4-aminopyrido[4,3-D]pyrimidine moieties (SKI-G-618 and SKI-O-85). One SYK inhibitor (SKI-G-618) exhibited moderate inhibitory activity against SYK, whereas the other inhibitor (SKI-O-85) exhibited a low inhibitory profile against SYK. Binding mode analysis indicates that a highly potent SYK inhibitor might be developed by modifying and optimizing the functional groups that interact with Leu377, Gly378, and Val385 in the G-loop and the nearby region in SYK. In agreement with our structural analysis, one of our SYK inhibitor (SKI-G-618) shows strong inhibitory activities on the β-hexosaminidase release and phosphorylation of SYK/Vav in RBL-2H3 cells. Taken together, our findings have important implications for the design of high affinity SYK inhibitors.

Keywords: cancer, crystal structure, rheumatoid arthritis, spleen tyrosine kinase; SYK

INTRODUCTION

Spleen tyrosine kinase (SYK) is a cytosolic non-receptor tyrosine kinase and is widely expressed at high levels in most hematopoietic cells, including mast cells, B lymphocytes, T lymphocytes, neutrophils, dendritic cells, and macrophages (MacFarlane and Todd, 2014; Singh et al., 2012). SYK activation in immune cells triggers cytokine release, B-cell involved inflammation, differentiation, proliferation, phagocytosis, Reactive oxygen species (ROS) production, cytoskeletal rearrangements, and survival through various immune recognition receptors (Lee et al., 2016; Mocsai et al., 2010; Shen et al., 2016; Singh et al., 2012; Thoma et al., 2014). Therefore, SYK is considered an attractive target for the treatment of multiple diseases such as arthritis and asthma. Moreover, constitutive SYK activation is fundamental to the proliferation and survival of some cancer types (Sharman et al., 2015). In contrast, SYK inhibition promotes apoptosis in many types of cancers, including B-cell lymphocytic leukemia, chronic lymphocytic leukemia, breast cancer, diffuse large B-cell lymphoma, follicular lymphoma, mantle cell lymphoma, pancreatic cancer, lung cancer, prostate cancer, retinoblastoma, ovarian cancer, and small cell lung cancer, implicating SYK as a potential anti-cancer target (Buchner et al., 2009; Cheng et al., 2011; Geahlen 2014; Ghotra et al., 2015; Lee

Received 15 September, 2017; revised 1 March, 2018; accepted 6 April, 2018; published online 12 June, 2018

eISSN: 0219-1032

et al., 2016; Prinos et al., 2011; Rinaldi et al., 2006).

To date, several distinct SYK inhibitors have been used for the treatment of autoimmune diseases and cancers, including fostamatinib (R406 or R788), entospletinib (GS-9973), cerdulatinib (PRT-062070), BAY61-3606, MK-8457, and TAK-659, which have been assessed in clinical trials (Coffey et al., 2014; Hoemann et al., 2016; Perova et al., 2014; Sharman et al., 2015; Shen et al., 2016). The reported SYK inhibitors bind with high affinity to the ATP binding pocket when SYK is in the active conformation. However, some of the developed SYK inhibitors have poor oral bioavailability and unsatisfactory physicochemical properties (Huang et al., 2017). Therefore, finding new SYK inhibitors with novel scaffolds or new therapeutic strategies are required to obtain successful drug candidates.

MATERIALS AND METHODS

Chemistry of SYK inhibitors (SKI-G-618 and SKI-O-85) and *in vitro* kinase assay

Two SYK inhibitors, SKI-G-618 [IUPAC name: 2-(4-hydroxypiperidin-1-yl)-4-((1-methyl-1H-indazol-5-yl)amino)pyrido[4,3-d]pyrimidin-5(6H)-one] and SKI-O-85 [IUPAC name: (1S,2S)-2-((4-((4-(methylsulfonyl)phenyl)amino)-5-oxo-5,6-dihydropyrido[4,3-d]pyrimidin-2-yl)amino)cyclohexan-1-aminium], were synthesized and characterized by Oscotec (Korea) and Genosco (USA). The chemical structures of SKI-G-618 and SKI-O-85 are shown in Fig. 2. The processes for their chemical synthesis and *in vitro* kinase assay protocols have been described elsewhere in detail (Choi et al., 2015; WO 2011/053861).

Protein expression and purification

To clone the kinase domain of the human SYK gene, the gene for the corresponding construct (residues 356-635) was amplified using PCR and cloned into the pVL1393 vector (BD Biosciences) using both *Bam*HI and *Eco*RI restriction sites. For efficient expression and purification of the recombinant protein, we added extra residues (MAL at the N-terminus and LEHHHHHHHH at the C-terminus) to the truncated SYK kinase domain construct. The recombinant proteins were expressed in Sf9 insect cells grown in Sf-900 II Serum-Free Media (Gibco) at 27℃. The cells were harvested by centrifugation 96 hours post-infection. The cells were lysed by sonication in lysis buffer (20 mM Tris-HCl at pH 7.9, 500 mM NaCl, 1 mM phenylmethylsulfonyl fluoride, and 10% (v/v) glycerol) supplemented with an EDTA-free protease inhibitor cocktail (Roche). After centrifugation of the crude lysate at approximately 36,000 *g* for 30 min, the supernatant was applied to a Ni^{2+}-NTA column (Qiagen) for affinity purification. After collecting the protein samples, 10 mM $MgCl_2$ and 5 mM DTT were added to the concentrated protein sample. The protein was further purified by size exclusion chromatography on a Superdex 75 prep-grade column (GE Healthcare) that was previously equilibrated with a buffer containing 10 mM HEPES at pH 7.5, 150 mM NaCl, 10 mM $MgCl_2$, 5 mM DTT, and 5% (v/v) glycerol. The highly purified protein fractions were pooled and concentrated to 10.6 mg/ml for crystallization using an Amicon Ultra-15 centrifugal filter unit (Millipore).

Crystallization and X-ray data collection

The SYK crystals were acquired by both the hanging-drop and sitting-drop vapor diffusion methods with a reservoir solution of 10-20% PEG 3350 and 100 mM Tris-HCl, pH 8.5 at 4℃ by mixing equal volumes (2 µl each) of the protein solution and the reservoir solution. To obtain crystals of the protein-inhibitor complexes, the protein was incubated with a 5-10-fold molar excess of the inhibitors for one hour at 4℃ before crystallization. To collect X-ray data, the crystals were soaked in a cryoprotectant solution containing the reservoir solution supplemented with 20% (v/v) glycerol before vitrification in liquid nitrogen. The SYK structural data were collected using an ADSC Quantum 315r CCD detector at the BL-5C experimental station (Pohang Light Source, Korea) and a Rigaku Jupiter 210 detector at the BL-26B1 experimental station (SPring-8, Japan). For each image, the crystal was rotated 1°, and the raw data were processed and scaled using programs in the HKL2000 suite (Otwinowski and Minor, 1997). The crystals belonged to the triclinic space group P1 or the monoclinic space group $P2_1$. Each asymmetric crystal unit contained two or one SYK monomers. Table 1 summarizes the data collection statistics.

Structure determination, refinement, and analysis

To determine the two SYK structures in complex with SKI-G-618 and SKI-O-85, the inhibitor-free SYK model (PDB code 4XG2) (Lee et al., 2016) was used as a search model to perform molecular replacement calculations (Vagin and Teplyakov, 2010). To refine the two SYK protein structures, we manually built the model and added water molecules using the program Coot (Emsley et al., 2010). The two inhibitors (SKI-G-618 and SKI-O-85) were assigned based on the *mFo* - *DFc* maps that were calculated using the model phases. The models were further refined with the programs Refmac (Vagin et al., 2004) and Phenix (Adams et al., 2010), including bulk solvent corrections. Five percent of the data were randomly set aside as a test set to calculate R_{free} (Brunger, 1992). The refined models showed excellent stereochemistry, which was evaluated using MolProbity (Chen et al., 2010). Structural deviation was calculated using Superpose (Krissinel and Henrick, 2004). The solvent-accessible surface areas and the detailed interactions were calculated using PIC (Tina et al., 2007) and LigPlot (Wallace et al., 1995), respectively. The refinement statistics are summarized in Table 1.

Protein data bank accession numbers

The atomic coordinates and structure factors for human SYK are deposited in the Protein Data Bank under accession codes 5Y5U (SKI-G-618) and 5Y5T (SKI-O-85).

Monitoring SYK/Vav phosphorylation

RBL-2H3 cells were seeded in 24-well plates (2×10^5 cells/well) and sensitized with 1 µg/ml anti-dinitrophenyl (DNP) IgE antibody. After overnight incubation, cells were incubated with SYK inhibitors prior to activation with DNP-BSA (1 ug/ml) for 1 h. RBL-2H3 cells were stimulated with DNP-BSA for 15 min and were lysed in RIPA buffer.

Table 1. Statistics for data collection, phasing, and model refinement

Data set	SKI-G-618	SKI-O-85
A. Data collection		
Space group	*P*1	$P2_1$
Unit cell length (Å)	a = 40.16, b = 42.01, c = 87.66	a = 40.27, b = 84.98, c = 42.14
Unit cell angle (°)	α = 79.83, β = 90.78, γ = 79.60	α = γ = 90.00, β= 99.59
X-ray wavelength (Å)	1.0000	1.0000
Resolution range (Å)	50.0-2.13 (2.17-2.13)	50.0-1.80 (1.83-1.80)
Total / unique reflections	59,164 / 28,936	171,549 / 24,430
Completeness (%)	94.3 (82.4)	93.9 (54.5)
$\langle I \rangle / \langle \sigma_I \rangle$	16.5 (2.3)	49.2 (3.5)
R_{merge} (%)[c]	6.9 (28.4)	5.2 (36.9)
B. Model refinement		
Resolution range (Å)	30.0-2.13	50.0-1.80
R_{work} / R_{free} (%)[d]	23.7 / 25.9	19.6 / 23.4
No. of non-hydrogen atoms / average B-factor (Å^2)		
Protein	4,249 / 40.8	2150 / 40.0
Water	67 / 35.8	162 / 45.1
Inhibitor	58 / 39.8	30 / 40.7
Wilson B-factor (Å^2)	34.1	31.3
R.m.s. deviations from ideal geometry		
Bond lengths (Å) / bond angles (°)	0.009 / 1.66	0.010 / 1.31
R.m.s. Z-scores		
Bond lengths / bond angles	0.675 / 0.694	0.337 / 0.556
Ramachandran plot (%)		
Favored / Outliers	97.0 / 0.2	97.0 / 0.0
Rotamer outliers (%)	2.6	1.3
PDB entry	5Y5U	5Y5T

[a] Values in parentheses refer to the highest resolution shell.
[c] $R_{merge} = \Sigma_h \Sigma_i | I(h)_i - \langle I(h) \rangle | / \Sigma_h \Sigma_i I(h)_i$, where $I(h)$ is the intensity of reflection h, Σ_h is the sum over all reflections, and Σ_i is the sum over i measurements of reflection h.
[d] $R = \Sigma | |F_{obs}| - |F_{calc}| | / \Sigma |F_{obs}|$, where R_{free} and R_{work} are calculated for a randomly chosen 5% of reflections that were not used for refinement and for the remaining reflections, respectively.

Equivalent amounts of protein were separated by NuPAGE 4-12% Bis-Tris Gel system (Invitrogen), and then transferred to polyvinylidene difluoride (PVDF) membranes. Membranes were probed with anti-phospho-SYK (Tyr525/ Tyr526) (Cell Signaling Technology), anti-phospho-Vav (Tyr174) (Santa Cruz Biotechnology), and anti-Actin antibodies (BD Biosciences). After incubation with the secondary antibody, the signal was detected by enhanced chemiluminescence with the Pierce ECL Plus Substrate (Thermo Scientific). For examination of the phosphorylation levels, the same whole cell lysates were resolved and immunoblotted.

β-hexosaminidase release inhibition assay

RBL-2H3 cells (rat basophilic leukemia) were obtained from the Korean Cell Line Bank (KCLB, Korea) and were maintained in Dulbecco's Modified Eagle Medium (DMEM) containing 10% FBS. RBL-2H3 cells were seeded in 96-well plates (4×10^4 cells/well) and washed with DMEM containing 10% FBS after 24 h. After 48 h, cells were washed with DMEM containing 10% FBS and treated with 0.1 μg/ml anti-dinitrophenyl (DNP) IgE (Sigma). After 20 h, IgE-sensitized cells were washed twice with Tyrode buffer (pH 7.7) and incubated with SYK inhibitors. After 30 mins, cells were treated with Tyrode buffer containing 0.1 μg/ml DNP-BSA (Merck) for 1 h. The released β-hexosaminidase in supernatants was measured by addition of *p*-nitrophenyl *N*-acetyl-*β*-D-glucosaminide at 405 nm after 1 h.

RESULTS AND DISCUSSION

Overall structures of SYK complexed with SKI-G-618 and SKI-O-85

We determined the crystal structures of the SKI-G-618-bound and SKI-O-85-bound SYK kinase domain (residues 356-635) at 2.13 and 1.80 Å resolutions, respectively (Figs. 1A and 1B) (Table 1). The refined models for the SKI-G-618-bound and SKI-O-85-bound SYK kinase domain contain 257-266 (monomers A and B) and 263 amino acid residues

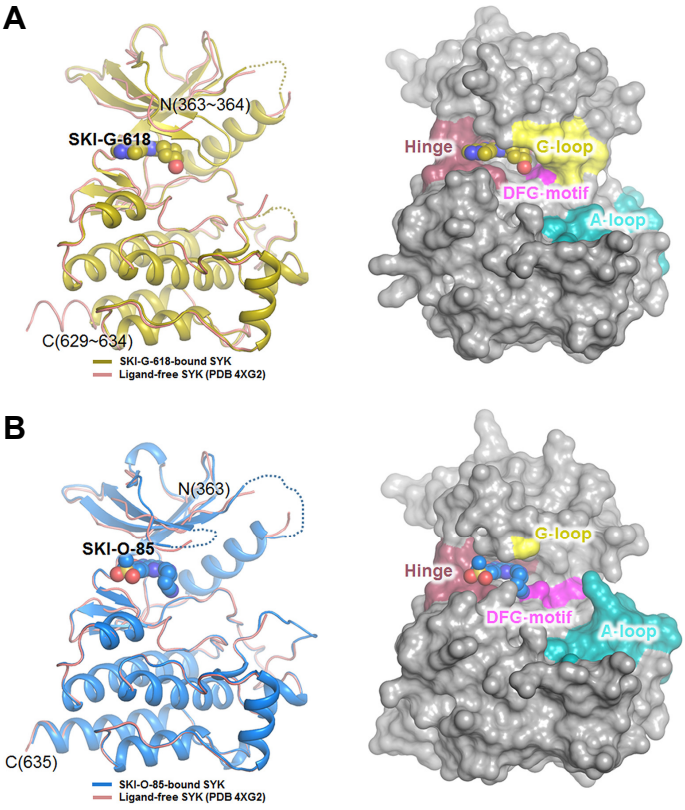

Fig. 1. The overall structures of SKI-G-618- and SKI-O-85-bound SYK. (A) A ribbon diagram and surface view of the SKI-G-618-bound SYK structure (yellow). The ligand-free structure (PDB 4XG2) is also depicted. The SYK inhibitor SKI-G-618 is drawn as a sphere model. In the surface view, the hinge region (residues 448-455), the glycine-rich loop (G-loop, residues 378-383), the DFG motif (residues 512-514), and the activation loop (A-loop, residues 520-534) are also indicated. (C) A ribbon diagram and surface view of the SKI-O-85-bound SYK structure (blue). The ligand-free structure is also depicted. The SYK inhibitor SKI-O-85 is drawn as a sphere model. The structures and surface diagram were drawn using PyMOL (DeLano WL, 2002, The PyMOL Molecular Graphics System; DeLano Scientific, Palo Alto, California).

with 67 and 162 water molecules in two and one monomers per asymmetric unit, respectively. In the SKI-G-618-bound model, the electron densities of residues Asn406 (Glu407)-Asp410 and Gln529-Trp534 were not visible because they were disordered. Therefore, we could not build a model for the corresponding residues. For the SKI-O-85-bound model, residues Ser379-Gly383 and Glu407-Pro411 were also not modeled because of their poor electron density. Interestingly, these disordered residues belong to the glycine-rich loop (G-loop or P-loop; Ser379-Gly383) and the activation loop (Gln529-Trp534), respectively.

The two SYK inhibitors (SKI-G-618 and SKI-O-85) were clearly observed in the ATP binding site of SYK, which is located between the N- and C-lobes and surrounded by the hinge region, the G-loop (residues 378-383), the DFG motif (residues 512-514), and the activation loop (A-loop; residues 520-534) (Fig. 1).

Discovery of two SYK inhibitors

To discover potent SYK inhibitors with a novel scaffold, we conducted a comprehensive chemoinformatic analysis combined with high-throughput screens using our in-house chemical library. Two SYK inhibitors (SKI-G-618 and SKI-O-85) are derivatives of 4-aminopyrido[4,3-d]pyrimidin-5(6*H*)-one, and SKI-G-618 contains two additional 1-methyl-1*H*-indazole and piperidin-4-ol [or (methylsulfonyl)benzene and (1*S*,2*S*)-2-aminocyclohexan-1-aminium in SKI-O-85] moieties (Fig. 2). The SYK inhibitor SKI-G-618 exhibits moderate inhibitory activity against SYK with an IC_{50} value of 17.7 nM, whereas the other SYK inhibitor, SKI-O-85, showed low SYK inhibitory activity with an IC_{50} value of 211 nM (Fig. 3). The binding free energies of SKI-G-618 and SKI-O-85, which were calculated using the Prime MMGBSA program in the Schrödinger program package, were -54.7 (kcals·mol^{-1}) and -55.8 (kcals·mol^{-1}), respectively. In this case, the calculated energy scores are not well correlated with the experimental IC_{50} values.

Analysis of the interactions between the inhibitors and SYK

The two SYK inhibitors (SKI-G-618 and SKI-O-85) in the SYK structures are similar to each other and have a horseshoe-like shape (Fig. 2). When we superimposed the two structures and compared the interactions between each inhibitor and the SYK structure, noticeable dissimilarity was observed both by manual inspection and the program LigPlot (Wallace et al., 1995).

In the SKI-G-618-bound structure, the 1-methyl-1*H*-indazole moiety in SKI-G-618 was recognized hydrophobically by Leu377, Gly454, and Pro455 (Fig. 4A). The piperidin-4-ol moiety of SKI-G-618 formed hydrophobic interactions with Gly378 and Val385. The core moiety of SKI-G-618, 4-aminopyrido[4,3-d]pyrimidin-5(6*H*)-one, formed two direct hydrophilic interactions with Ala451 (2.7 Å) and Glu449 (2.8 Å) and formed multiple hydrophobic interactions with Val385, Ala400, Val433, Met448, and Leu501 (Fig. 4A). In the SKI-O-85-bound structure, both the (methylsulfonyl)benzene moiety and the (1*S*,2*S*)-2-aminocyclohexan-1-aminium moiety

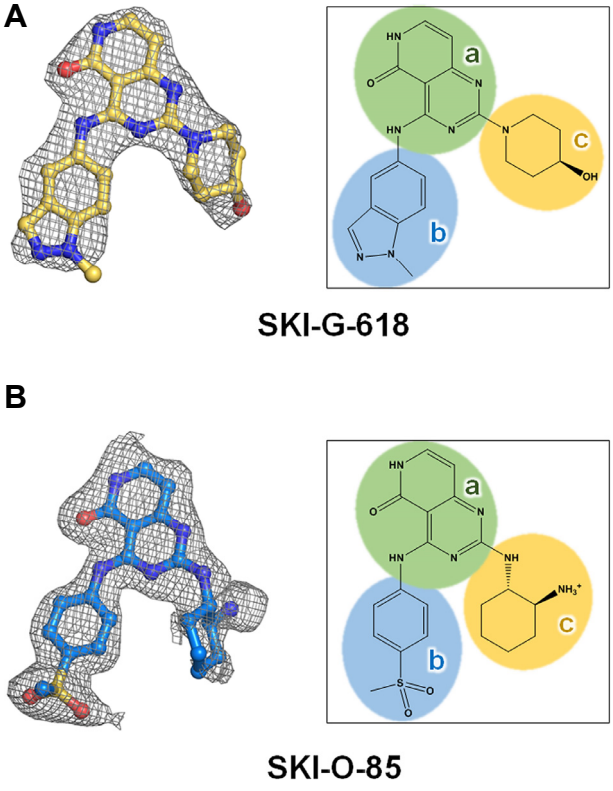

Fig. 2. The SKI-G-618 and SKI-O-85 structures analyzed in this study. (A) m*Fo* - D*Fc* electron density maps (in gray mesh and contoured at 2.0σ) of SKI-G-618 are depicted in the left panel. The chemical structure of SKI-G-618, 2-(4-hydroxypiperidin-1-yl)-4-((1-methyl-1H-indazol-5-yl)amino)pyrido[4,3-d]pyrimidin-5(6H)-one, is presented in the right panel. The three moieties are also indicated as (a) 4-aminopyrido[4,3-d]pyrimidin-5(6*H*)-one, (b) 1-methyl-1*H*-indazole, and (c) piperidin-4-ol, which are represented in green, blue, and yellow, respectively. (B) The m*Fo* - D*Fc* electron density maps (in gray mesh and contoured at 1.2σ) of SKI-O-85 are depicted in the left panel. The chemical structure of SKI-O-85, (1S,2S)-2-((4-((4-(methylsulfonyl)phenyl)amino)-5-oxo-5,6-dihydropyrido[4,3-d]pyrimidin-2-yl)amino)cyclohexan-1-aminium, is presented in the right panel. The three moieties are also indicated as (a) 4-aminopyrido[4,3-d]pyrimidin-5(6*H*)-one, (b) (methylsulfonyl)benzene, and (c) (1*S*,2*S*)-2-aminocyclohexan-1-aminium, which are represented in green, blue, and yellow, respectively.

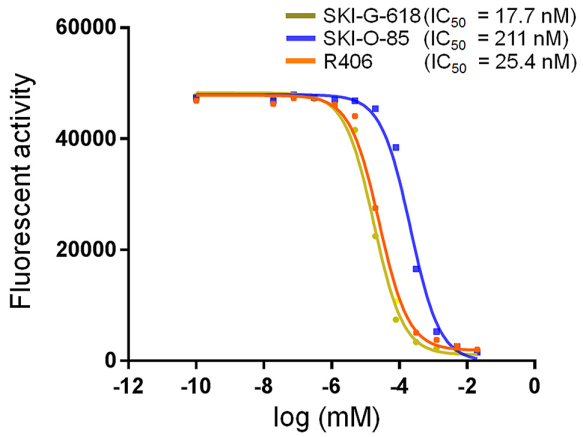

Fig. 3. The kinase assay results (IC_{50}) of SKI-G-618 and SKI-O-85. The experiments were performed as separate triplicate trials. The assay was also performed with the reference compound fostamatinib (R406).

in SKI-O-85 interacted hydrophobically with Gly454 and Pro455. The (1*S*,2*S*)-2-aminocyclohexan-1-aminium moiety formed additional hydrophilic interactions with Arg498 (3.5 Å) and Asp512 (2.9 Å) (Fig. 4B). The 4-aminopyrido[4,3-d]pyrimidin-5(6*H*)-one moiety in SKI-O-85 formed two direct hydrophilic interactions with Ala451 (2.9 Å) and Glu449 (2.7 Å) and formed hydrophobic interactions with Ala400, Val433, Met448, and Leu501, similar to the interactions observed for the identical moiety in SKI-G-618 (Fig. 4B). The residues that bind to the two SYK inhibitors are positioned in the G-loop (Gly378), the G-loop neighboring region (Leu377 and Val385), the gatekeeper (Met448), the hinge region (Gly454, and Pro455), the area near the hinge region (Ala500 on β4 and Leu501 on β8), the area between the hinge region and the DFG motif (Val433), the DFG motif (Asp512), and the loop between β8 and α4 (Arg498) (Fig. 4). Unlike SKI-G-618, SKI-O-85 interacts with Asp512 in the DFG motif, which does not allow any structural rearrangement in the DFG motif of the kinase (Liu and Gray, 2006). However, both the SKI-O-85- and SKI-G-618-bound SYK structures adopt the active DFG-in conformation, regardless of the interaction between the ligand and Asp512 residue. The electron densities for the DFG motif are clearly observed in both SKI-G-618- and SKI-O-85-bound SYK structures. All of these structural data indicate that our two SYK inhibitors are type I inhibitors (Lovering et al., 2012). The binding modes of our SKI-G-618 and SKI-O-85 to SYK are nearly identical to the adenosine moiety in ANP except for the extended triphosphate moiety (Fig. 4C).

Comparison of the two SYK inhibitors SKI-G-618 and SKI-O-85

Although SKI-G-618 and SKI-O-85 have identical cores of 4-aminopyrido[4,3-d]pyrimidin-5(6*H*)-one, their SYK inhibitory activity is quite different and likely is derived from the chemical diversity of the two other groups that covalently link to the 4-aminopyrido[4,3-d]pyrimidin-5(6*H*)-one moiety. Overall, the 4-aminopyrido[4,3-d]pyrimidin-5(6*H*)-one moiety in SKI-G-618 has more interactions with the G-loop and its nearby region (Leu377, Gly378, and Val385), whereas this group in SKI-O-85 did not interact with the corresponding residues. Instead, direct hydrophilic interactions between the (1*S*,2*S*)-2-aminocyclohexan-1-aminium moiety of SKI-O-85 and SYK were observed, whereas similar interactions between the equivalent moiety and SYK were not seen in SKI-G-618. This might indicate that more hydrophilic interactions of the (1*S*,2*S*)-2-aminocyclohexan-1-aminium moiety in SKI-O-85 (or piperidin-4-ol moiety in SKI-G-618) do not

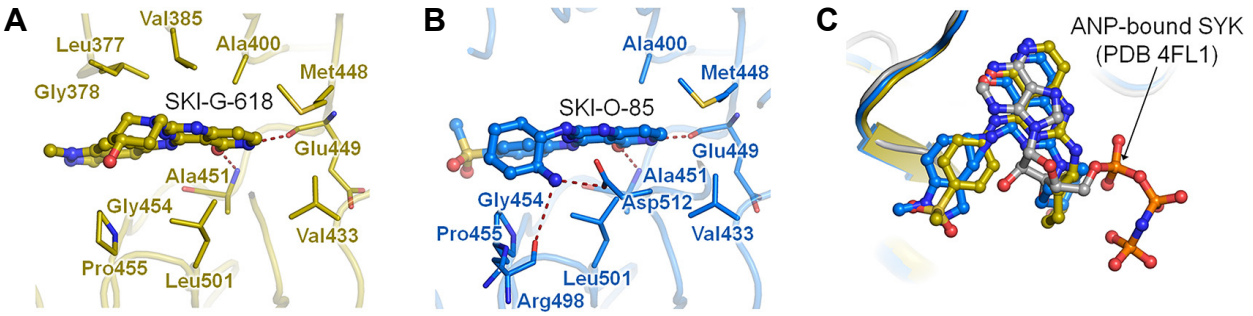

Fig. 4. The binding modes of two SYK inhibitors (SKI-G-618 and SKI-O-85). (A) Interactions between SKI-G-618 and the residues in the SYK active site. The interacting residues are colored in yellow. (B) Interactions between SKI-O-85 and residues in the SYK active site. The interacting residues are colored in blue. The direct hydrophilic interactions are indicated by red dotted lines in the figures. (C) The structural superposition of the inhibitor-bound SYK structures and the ANP-bound SYK structure (gray).

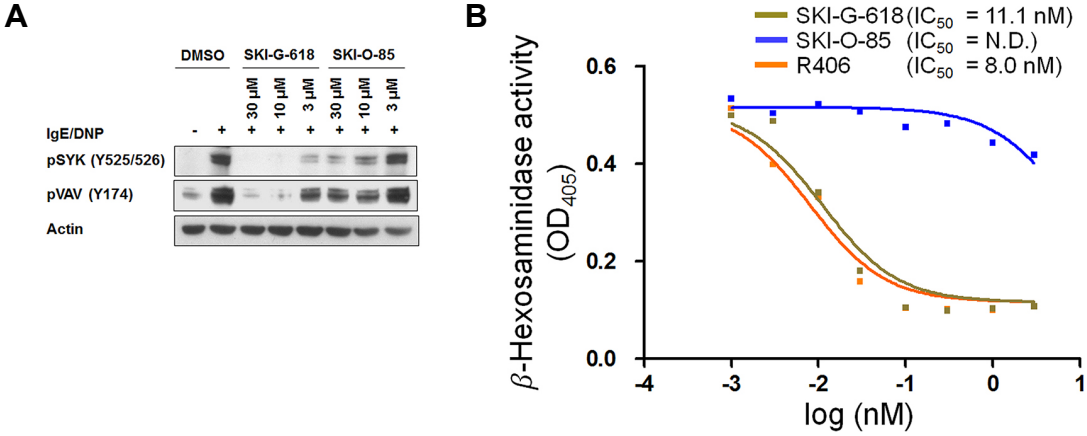

Fig. 5. Effects of two SYK inhibitors (SKI-G-618 and SKI-O-85) on phosphorylation of SYK/Vav and release of β-hexosaminidase. (A) Western blot analysis showing inhibition of active SYK/Vav in RBL-2H3 cells treated with SKI-G-618 and SKI-O-85. All assays were performed as separate triplicate trials with the reference compound fostamatinib (R406). (B) Inhibitory activities of SKI-G-618 and SKI-O-85 on the β-hexosaminidase release inhibition.

largely contribute to the affinity of the SYK inhibitor. Furthermore, it might show that the interactions between the inhibitor and residues in the DFG motif do not largely affect the level of inhibition achieved. For SYK inhibitors, interactions with four amino acid residues (Met450, Leu453, Pro455, and Asn457) in SYK were the most challenging during the optimization of SYK inhibitors because they are present in less than 5% of all kinases (Lucas et al., 2012). Considering the hydrophobic interaction between SKI-G-618 (or SKI-O-85) and Pro455, the structural information and binding mode analysis of our two bound SYK structures might improve the rational drug design of SYK inhibitors.

SKI-G-618 inhibits IgE-dependent cellular signaling

Activated SYK (phospho-SYK) phosphorylates Vav that belongs to a guanosine nucleotide exchange factor for the Rac family of GTP binding proteins (Das, 2010). Therefore, we examined whether our two SYK inhibitors arrest activation of SYK and Vav in living cells. In RBL-2H3 cell, it was clearly shown that SKI-G-618 strongly inhibits phosphorylation of both SYK and Vav, whereas SKI-O-85 was found to weakly inhibit SYK and Vav (Fig. 5). As the concentration of SKI-G-618 is increased, activation of SYK and Vav are strongly decreased. However, SKI-O-85 does not show a large decrease of SYK and Vav activation. In addition, when we performed β-hexosaminidase release inhibition assay, SKI-G-618 was also shown to inhibit the β-hexosaminidase release in a stong way (Fig. 5). Unlike SKI-G-618, SKI-O-85 did not show a strong inhibitory activity against the β-hexosaminidase release. Generally, β-hexosaminidase is regarded as a general biomarker of degranulation and a hallmark characteristic of allergic reactions caused by allergen exposure (Tang et al., 2015). Therefore, this experimental result indicates that SKI-G-618 possesses strong anti-allergic effect on IgE-mediated inflammatory responses.

In conclusion, we discovered two SYK inhibitors (SKI-G-618 and SKI-O-85) and performed comparative studies on two inhibitor-bound SYK structures. The binding mode anal-

ysis indicates that a highly potent SYK inhibitor might be developed by optimizing the functional groups that interact with the G-loop and the neighboring region in SYK. In agreement with our structural analysis, one of our SYK inhibitors (SKI-G-618) shows strong inhibitory activities on the β-hexosaminidase release and phosphorylation of SYK/Vav.

Taken together, the structural information from our SYK-inhibitor complexes will be helpful for the structure-based optimization of effective inhibitors.

ACKNOWLEDGMENTS

We thank the beamline staff at the Pohang Light Source (Korea, BL-5C) and at SPring-8 (Japan, BL44XU and BL26B1) for assistance with the X-ray diffraction experiments. This work was supported by the Korea Ministry of Science and ICT through the National Research Foundation of Korea (NRF-2015R1A2A2A01003004 to BIL; NRF-2016R1C1B2014609 to SJL, NRF-2017R1D1A1B03034433 to SMB) and by National Cancer Research Grants (1610020 to BIL).

REFERENCES

Adams, P.D., Afonine, P.V., Bunkoczi, G., Chen, V.B., Davis, I.W., Echols, N., Headd, J.J., Hung, L.W., Kapral, G.J., Grosse-Kunstleve, R.W., et al. (2010). PHENIX: a comprehensive Python-based system for macromolecular structure solution. Acta Crystallogr. D Biol. Crystallogr. *66*, 213-221.

Brunger, A.T. (1992). Free R value: a novel statistical quantity for assessing the accuracy of crystal structures. Nature *355*, 472-475.

Buchner, M., Fuchs, S., Prinz, G., Pfeifer, D., Bartholome, K., Burger, M., Chevalier, N., Vallat, L., Timmer, J., Gribben, J.G., et al. (2009). Spleen tyrosine kinase is overexpressed and represents a potential therapeutic target in chronic lymphocytic leukemia. Cancer Res. *69*, 5424-5432.

Chen, V.B., Arendall, W.B., 3rd, Headd, J.J., Keedy, D.A., Immormino, R.M., Kapral, G.J., Murray, L.W., Richardson, J.S. and Richardson, D.C. (2010). MolProbity: all-atom structure validation for macromolecular crystallography. Acta Crystallogr. D Biol. Crystallogr. *66*, 12-21.

Cheng, S.H., Coffey, G., Zhang, X.H.N., Shaknovich, R., Song, Z.B., Lu, P., Pandey, A., Melnick, A.M., Sinha, U. and Wang, Y.L. (2011). SYK inhibition and response prediction in diffuse large B-cell lymphoma. Blood *118*, 6342-6352.

Choi, J.S., Hwang, H.J., Kim, S.W., Lee, B.I., Lee, J., Song, H.J., Koh, J.S., Kim, J.H. and Lee, P.H. (2015). Highly potent and selective pyrazolylpyrimidines as Syk kinase inhibitors. Bioorg. Med. Chem. Lett. *25*, 4441-4446.

Coffey, G., Betz, A., DeGuzman, F., Pak, Y., Inagaki, M., Baker, D.C., Hollenbach, S.J., Pandey, A. and Sinha, U. (2014). The novel kinase inhibitor PRT062070 (Cerdulatinib) demonstrates efficacy in models of autoimmunity and B-cell cancer. J. Pharmacol. Exp. Ther. *351*, 538-548.

Das J. (2010) Activation or tolerance of natural killer cells is modulated by ligand quality in a nonmonotonic manner. Biophys. J. *99*, 2028-2037

Emsley, P., Lohkamp, B., Scott, W.G. and Cowtan, K. (2010). Features and development of Coot. Acta Crystallogr. D Biol. Crystallogr. *66*, 486-501.

Geahlen, R.L. (2014). Getting Syk: spleen tyrosine kinase as a therapeutic target. Trends Pharmacol. Sci. *35*, 414-422.

Ghotra, V.P.S., He, S.N., van der Horst, G., Nijhoff, S., de Bont, H., Lekkerkerker, A., Janssen, R., Jenster, G., van Leenders, G.J.L.H., Hoogland, A.M.M., et al. (2015). SYK Is a candidate kinase target for the treatment of advanced prostate cancer. Cancer Res. *75*, 230-240.

Hoemann, M., Wilson, N., Argiriadi, M., Banach, D., Burchat, A., Calderwood, D., Clapham, B., Cox, P., Duignan, D.B., Konopacki, D., et al. (2016). Synthesis and optimization of furano[3,2-d]pyrimidines as selective spleen tyrosine kinase (Syk) inhibitors. Bioorg. Med. Chem. Lett. *26*, 5562-5567.

Huang, Y.H., Zhang, Y.J., Fan, K.X., Dong, G.Q., Li, B.H., Zhang, W.N., Li, J. and Sheng, C.Q. (2017). Discovery of new Syk inhibitors through structure-based virtual screening. Bioorg. Med. Chem. Lett. *27*, 1776-1779.

Krissinel, E. and Henrick, K. (2004). Secondary-structure matching (SSM), a new tool for fast protein structure alignment in three dimensions. Acta Crystallogr. D Biol. Crystallogr. *60*, 2256-2268.

Lee, S.J., Choi, J.S., Han, B.G., Kim, H.S., Song, H.J., Lee, J., Nam, S., Goh, S.H., Kim, J.H., Koh, J.S., et al. (2016). Crystal structures of spleen tyrosine kinase in complex with novel inhibitors: structural insights for design of anticancer drugs. FEBS J. *283*, 3613-3625.

Liu, Y. and Gray, N.S. (2006). Rational design of inhibitors that bind to inactive kinase conformations. Nat. Chem. Biol. *2*, 358-364.

Lovering, F., McDonald, J., Whitlock, G.A., Glossop, P.A., Phillips, C., Bent, A., Sabnis, Y., Ryan, M., Fitz, L., Lee, J., et al. (2012). Identification of type-II inhibitors using kinase structures. Chem. Biol. Drug. Des. *80*, 657-664.

Lucas, M.C., Goldstein, D.M., Hermann, J.C., Kuglstatter, A., Liu, W., Luk, K.C., Padilla, F., Slade, M., Villasenor, A.G., Wanner, J., et al. (2012). Rational design of highly selective spleen tyrosine kinase inhibitors. J. Med. Chem. *55*, 10414-10423.

MacFarlane, L.A. and Todd, D.J. (2014). Kinase inhibitors: the next generation of therapies in the treatment of rheumatoid arthritis. Int. J. Rheum. Dis. *17*, 359-368.

Mocsai, A., Ruland, J. and Tybulewicz, V.L. (2010). The SYK tyrosine kinase: a crucial player in diverse biological functions. Nat. Rev. Immunol. *10*, 387-402.

Otwinowski, Z. and Minor, W. (1997). Processing of X-ray diffraction data collected in oscillation mode. Method. Enzymol. *276*, 307-326.

Perova, T., Grandal, I., Nutter, L.M., Papp, E., Matei, I.R., Beyene, J., Kowalski, P.E., Hitzler, J.K., Minden, M.D., Guidos, C.J., et al. (2014). Therapeutic potential of spleen tyrosine kinase inhibition for treating high-risk precursor B cell acute lymphoblastic leukemia. Sci. Transl. Med. *6*, 236ra262.

Prinos, P., Garneau, D., Lucier, J.F., Gendron, D., Couture, S., Boivin, M., Brosseau, J.P., Lapointe, E., Thibault, P., Durand, M., et al. (2011). Alternative splicing of SYK regulates mitosis and cell survival. Nat. Struct. Mol. Biol. *18*, 673-679.

Rinaldi, A., Kwee, I., Taborelli, M., Largo, C., Uccella, S., Martin, V., Poretti, G., Gaidano, G., Calabrese, G., Martinelli, G., et al. (2006). Genomic and expression profiling identifies the B-cell associated tyrosine kinase Syk as a possible therapeutic target in mantle cell lymphoma. Brit. J. Haematol. *132*, 303-316.

Sharman, J., Hawkins, M., Kolibaba, K., Boxer, M., Klein, L., Wu, M., Hu, J., Abella, S. and Yasenchak, C. (2015) An open-label phase 2 trial of entospletinib (GS-9973), a selective Syk inhibitor, in chronic lymphocytic leukemia. Blood *125*, 2336-2343.

Shen, J.Y., Li, X.K., Zhang, Z., Luo, J.F., Long, H.Y., Tu, Z.C., Zhou, X.P., Ding, K. and Lu, X.Y. (2016). 3-aminopyrazolopyrazine derivatives as spleen tyrosine kinase inhibitors. Chem. Biol. Drug. Des. *88*, 690-698.

Singh, R., Masuda, E.S. and Payan, D.G. (2012). Discovery and

development of spleen tyrosine kinase (SYK) inhibitors. J. Med. Chem. *55*, 3614-3643.

Tang, F., Chen, F., Ling, X., Huang, Y., Zheng, X., Tang, Q. and Tan, X. (2015). Inhibitory effect of methyleugenol on IgE-mediated allergic inflammation in RBL-2H3 cells. Mediators Inflamm. *463530*, 1-9.

Thoma, G., Blanz, J., Buhlmayer, P., Druckes, P., Kittelmann, M., Smith, A.B., van Eis, M., Vangrevelinghe, E., Zerwes, H.G., Che, J.J., et al. (2014). Syk inhibitors with high potency in presence of blood. Bioorg. Med. Chem. Lett. *24*, 2278-2282.

Tina, K.G., Bhadra, R. and Srinivasan, N. (2007). PIC: Protein Interactions Calculator. Nucleic Acids Res. *35*, W473-W476.

Vagin, A. and Teplyakov, A. (2010). Molecular replacement with MOLREP. Acta crystallographica. Section D, Biological crystallography *66*, 22-25.

Vagin, A.A., Steiner, R.A., Lebedev, A.A., Potterton, L., McNicholas, S., Long, F. and Murshudov, G.N. (2004). REFMAC5 dictionary: organization of prior chemical knowledge and guidelines for its use. Acta Crystallogr. D Biol. Crystallogr. *60*, 2184-2195.

Wallace, A.C., Laskowski, R.A. and Thornton, J.M. (1995). Ligplot - a program to generate schematic diagrams of protein ligand interactions. Protein Eng. *8*, 127-134.